International Journal of Minerals, Metallurgy and Materials
Volume 22, Number 7, July 2015, Page 729
DOI: 10.1007/s12613-015-1128-5

Electrochemical investigation on the hydrogen permeation behavior of 7075-T6 Al alloy and its influence on stress corrosion cracking

Chuan-bo Zheng[1,2], *Bing-hao Yan*[1], *Ke Zhang*[3], *and Guo Yi*[1]

1) School of Materials Science and Engineering, Jiangsu University of Science and Technology, Zhenjiang 212003, China

2) Key Laboratory of Marine Environmental Corrosion and Bio-fouling, Institute of Oceanology, Chinese Academy of Sciences, Qingdao 266071, China

3) China Petroleum Pipeline Bureau, Langfang 065000, China

(Received: 15 September 2014; revised: 18 November 2014; accepted: 1 March 2015)

Abstract: The hydrogen permeation behavior and stress corrosion cracking (SCC) susceptibility of precharged 7075-T6 Al alloy were investigated in this paper. Devanthan–Stachurski (D-S) cell tests were used to measure the apparent hydrogen diffusivity and hydrogen permeation current density of specimens immersed in 3.5wt% NaCl solution. Electrochemical experiment results show that the SCC susceptibility is low during anodic polarization. Both corrosion pits and hydrogen-induced cracking are evident in scanning electron microscope images after the specimens have been charging for 24 h.

Keywords: aluminum alloys; hydrogen permeation; hydrogen embrittlement; stress corrosion cracking

1. Introduction

Stress corrosion cracking (SCC) can cause the significant service failures of engineering materials in the aeronautical, nuclear, and petrochemical industries. 7075 aluminum alloy, as a representative of 7XXX-series aluminum alloy, is widely used as an aircraft structural material because of its high strength and low density. However, this alloy is susceptible to various forms of corrosion in chloride environments, such as SCC, pitting corrosion, intergranular corrosion, and exfoliation corrosion. Metal oxidation is well recognized as being associated with the reduction of hydrogen ions in aqueous acid solutions. The generated hydrogen permeates into the metal and accumulates around the corrosion sites [1–2].

SCC of 7075 aluminum represents a continuing problem in the aerospace industry. Therefore, SCC of 7075 aluminum alloys has been extensively investigated, especially in aqueous chloride solutions. Jones *et al.* [3] and Najjar *et al.* [4] proposed a model involved both hydrogen embrittlement (HE) and anodic dissolution. Nevertheless, the research on the mechanism of SCC in 7075 aluminum should be investigated further [5–11].

Numerous investigations have been conducted to study the effects of hydrogen on the mechanical properties of Al alloys [12–15]. However, the literature contains little information with respect to the hydrogen permeation effect on the SCC of Al alloys, because measuring the hydrogen permeation current of Al alloys is inherently difficult as a consequence of the oxidation film formed on their surface. In addition, the deposition of pure Pd or Ni film onto Al alloy surfaces is also difficult. A Devanthan–Stachurski (D-S) cell provides a quick and convenient method to measure the hydrogen permeation through a metal; however, a literature search revealed that the results obtained using D-S methods could not reproduced when it was applied to Al alloys [16–20].

In this paper, hydrogen permeation into 7075-T6 Al alloy was studied using a D-S cell. The specimen was coated with a thin layer of Ni via a magnetron sputtering method. In addition, the SCC of 7075-T6 Al alloy was studied using slow strain rate tests (SSRTs) after the samples were subjected to cathodic charging for various times.

Corresponding author: Chuan-bo Zheng E-mail: 15952802516@139.com

© University of Science and Technology Beijing and Springer-Verlag Berlin Heidelberg 2015

2. Experimental

Chemical composition of the commercial 7075-T6 high-strength aluminum alloy is given in Table 1.

Table 1. Chemical composition of the 7075 aluminum alloy

wt%

Cu	Mg	Zn	Si	Fe	Cr	Others	Al
1.3	2.5	6.2	0.4	0.5	0.18	0.65	Balance

2.1. Hydrogen permeation tests

For the hydrogen permeation tests, disc plate specimens with 40 mm in diameter and 0.4 mm in thickness were used as the working electrode; both sides of the specimen were coated with a thin layer of Ni via a magnetron sputtering method; the working pressure was 0.3 Pa, and the sputtering power was 40 W. Before the tests, the specimens were carefully cleaned with alcohol and acetone using an ultrasonic bath and then dried with cold air. Ouyang *et al.* [20] showed that a hydrogen permeation current could be detected in an unplated specimen; however, the current density was approximately 10% that of a Ni-plated specimen. Zheng *et al.* [21] studied the effects of the Ni-coating thickness on the hydrogen permeation current. Their results revealed that hydrogen atoms could be thoroughly oxidized when the Ni coating thickness was between 180 nm and 220 nm; however, they also observed that the hydrogen permeation current decreased when the thickness exceeded 220 nm.

A D-S cell was used to study the hydrogen penetration current through the specimen. Fig. 1 shows the experimental setup used for the hydrogen permeation tests.

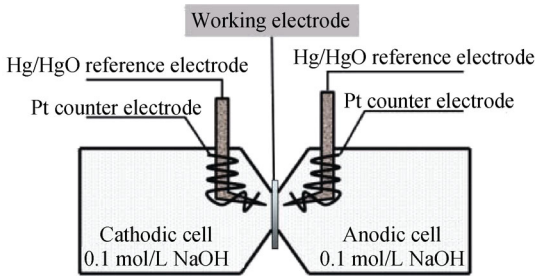

Fig. 1. Schematic illustration of the experimental setup used for hydrogen permeation tests.

For hydrogen permeation tests in 3.5wt% NaCl solution, one side of the cell was filled with 0.1 mol/L NaOH. Prior to the tests, the specimens were polarized potentiostatically at 100 mV vs. HgO/Hg/0.1 mol/L NaOH until the passivation current density was less than 0.1 μA/cm^2. Then, 3.5wt% NaCl solution was added to the other side of the cell. The tests were conducted at 25°C. To verify the reproducibility of results, the hydrogen permeation tests were performed in triplicate using three specimens with different Ni-coating thicknesses. In this paper, the Ni coating thickness was calculated on the basis of the weight gain of each specimen before and after the Ni coating was deposited. The weight gains were approximately 1.9, 2.2, and 2.5 mg, for which the calculated thicknesses were approximately 190, 210, and 230 nm, respectively.

2.2. Electrochemical experiments

The electrochemical measurements were performed using a Gamry Reference 600 electrochemical workstation and a three-electrode cell. The 7075-T6 alloy electrode served as the working electrode (WE), platinum foil was used as the counter electrode (CE), and a Ag/AgCl electrode was used as the reference electrode (RE). The open corrosion potential (OCP), potentiodynamic polarization curves, and fast-slow polarization curves of 7075-T6 Al alloy in 3.5wt% NaCl solution were measured.

2.3. Slow strain rate tests

SCC susceptibility was evaluated on the basis of slow strain rate tests (SSRTs). The SSRT experimental specimen is shown in Fig. 2.

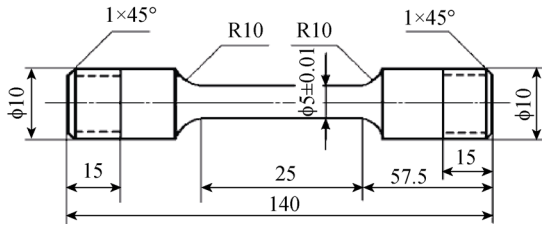

Fig. 2. Schematic illustration of the specimen used for SSRTs (unit: mm).

Each specimen was polished along the tensile direction with 1000-grit emery paper, degreased in acetone, and washed with distilled water immediately before being tested. Before each SSRT test, the specimen was pre-charged with a charging current density of −3 mA/cm^2 in 3.5wt% NaCl solution for 6, 12, or 24 h. SSRT tests were conducted after the cathodic charging was complete. The specimens were completely immersed in aqueous 3.5wt% NaCl solution during the whole test. All tests were performed in triplicate.

3. Results and discussion

3.1. Hydrogen permeation tests

To estimate the apparent hydrogen diffusivity of 7075 Al

alloy, hydrogen permeation tests in 0.1 mol/L NaOH solution using a –3 mA/cm^2 charging current density were carried out, and the results are shown in Fig. 3.

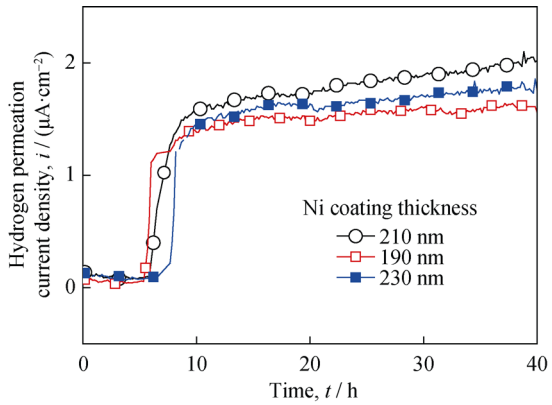

Fig. 3. Hydrogen permeation current density of 7075 Al alloy in 0.1 mol/L NaOH solution with a charging current density of –3 mA/cm^2, where all the electrolyte cells are filled with 0.1 mol/L NaOH and the cathodic cell is charged at a current density of –3 mA/cm^2.

To analyze the apparent hydrogen diffusivity, a time-lag method was employed as the following [22]:

$$D = \frac{L^2}{6t_L} \tag{1}$$

where t_L corresponds to the time point on the permeation curve at which $i_t = 0.63\ i_s$, where i_t is the instantaneous hydrogen permeation current density and i_s is the steady hydrogen permeation current density, L the thickness of specimen, and D the apparent hydrogen diffusivity.

The hydrogen permeation rate, V (mol/(cm·s)) was estimated according to Eq. (2).

$$V = J_s \cdot L = i_s \cdot L / F \tag{2}$$

where J_s is the steady-state hydrogen permeation flux, mol/(cm^2·s); i_s the steady state current density, A/cm^2; and F the Faraday's constant.

The hydrogen solubility in the specimens, C (mol/cm^3), is defined by Eq. (3).

$$C = J_s \cdot L / D = i_s \cdot L / FD \tag{3}$$

The calculation results were shown as $D = 1.3 \times 10^{-10}$ m^2/s, $V = 2.1 \times 10^{-10}$ mol/(cm·s), and $C = 0.56$ mol/cm^3. Numerous researchers have investigated the hydrogen permeation diffusivity of Al alloys, but little consensus has been reached. Gest and Troiano [23] measured the hydrogen permeation coefficient of AA7075-T651 using a D-S cell and obtained a D value of approximately 2×10^{-13} m^2/s; in addition, they demonstrated HE of Al alloys by observing the promotion effect of anodic polarization on the hydrogen permeation rate. Onuchukwu and Trasatti [18] studied the hydrogen permeation behavior of pure AA1060 Al and obtained a D value of approximately 3×10^{-9} m^2/s. Kupka [24] used a D-S cell to measure the hydrogen permeation diffusivity of Fe-40at% Al alloy and obtained a D-value of approximately 5.05×10^{-10} m^2/s. In this paper, three specimens with different Ni coating thicknesses (190, 210, and 230 nm) were tested. The hydrogen permeation current density was similar in all three experiments. Similar results have been reported by Kupka *et al.* [24] and Onuchukwu and Trasatti [18].

Fig. 4 shows the hydrogen permeation current density of 7075 Al alloy with different Ni coating thicknesses (190, 210, and 230 nm) in 3.5% NaCl solution.

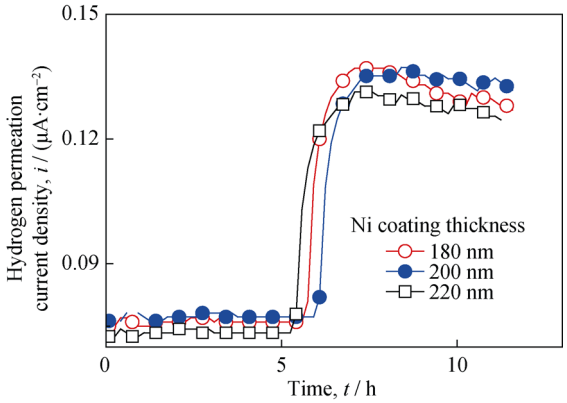

Fig. 4. Hydrogen permeation current density of 7075 Al alloy with different Ni coating thicknesses in 3.5wt% NaCl solution, where the cathodic cell is filled with 3.5wt% NaCl solution and no charging current is used.

The results show that the current density is small; thus, hydrogen atoms could permeate into the Al alloy during the corrosion process. The hydrogen permeation current density tends to decrease over time. After the specimens were immersed into the 3.5wt% NaCl solution for several hours, the corrosion products were formed; the corrosion product film blocked hydrogen-ion diffusion from the solution to the metal surface. Although no direct evidence was obtained to prove this viewpoint for the Al alloy, several researchers have previously demonstrated its validity in the case of steel [15,20,25]. The relationship between the hydrogen permeation current density (i_s) and the hydrogen solubility (C) is shown in Eq. (3). In this equatiom, L, F, and D are constant and the relation between i_s and C is linear. The surface area is increased upon the formation of corrosion products. It is assumed that, if the total hydrogen amount (generated by corrosion reactions) keeps steady, the hydrogen concentration decreases with time. Thus, the hydrogen permeation current density decreases with time.

3.2. Electrochemical experiments

The OCP was measured in 3.5wt% NaCl solution without loading; the results are shown in Fig. 5.

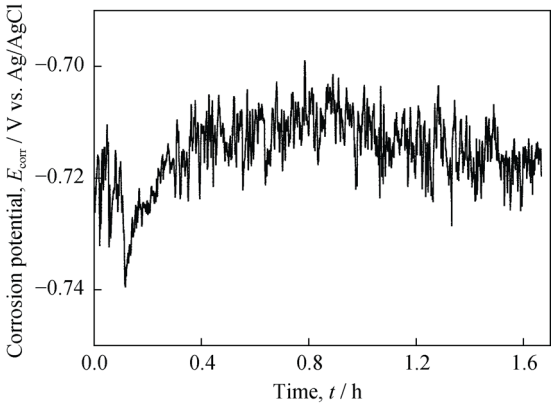

Fig. 5. OCP of 7075-T6 Al alloy in 3.5wt% NaCl solution, where an Ag/AgCl electrode and Pt are used as the reference and counter electrodes, respectively.

Some fluctuations are observed in the corrosion potential measured with the specimens immersed in 3.5wt% NaCl solution, as shown in Fig. 5. Passivation and pitting corrosion occurred after the specimens were immersed into the 3.5wt% NaCl solution. Chen *et al.* [26] investigated the potential fluctuations of 7075 aluminum alloy under thin electrolyte layers and observed that the initiation of pitting occurred after 6 h. This result indicated that a competition mechanism existed between passivation and pitting corrosion.

Fig. 6 shows the potentiodynamic polarization curve of 7075-T6 Al alloy in 3.5wt% NaCl solution. The potential was scanned from cathodic to anodic at a scan rate of 0.1 mV/s. In the cathodic branch, oxygen reduction to OH^- ions occurs at potentials lower than −1.1 V vs. Ag/AgCl because of water electrolysis. When the potential is anodically scanned, neither an active current peak nor a potential of complete passivation (Flade potential) is observed, indicating that the alloy is passivated immediately. The passive region covers a relatively broad range of potential from approximately −0.5 V to 1.2 V vs. Ag/AgCl. These results were similar to those of Grzegorz's results [27].

According to Parkins's fast-slow polarization method, two polarization curves can be measured by a fast scan rate (approximately 1000 mV/min) and a slow scan rate (approximately 10 mV/min) to control the passivation film growth velocity. The difference in the anode polarization current density can indicate the potential region of SCC susceptibility. SCC occurs in the activation-passivation marginal zone, where activation and passivation occur in this zone together [28]. The potential region of SCC susceptibility can be measured from anodic polarization curves. Fig. 7 shows the fast-slow polarization curves of 7075-T6 Al alloy in 3.5wt% NaCl solution.

As shown in Fig. 7, the difference in the scanning region is not obvious, which suggests that the SCC susceptibility of specimens is low from approximately −0.75 V to −0.16 V vs. Ag/AgCl. This difference increases with increasing potential, indicating that the anodic dissolution dominates the SCC mechanism under strong anodic polarization conditions.

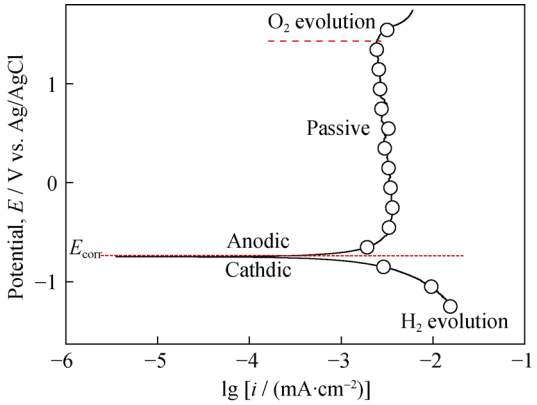

Fig. 6. Potentiodynamic polarization curves of 7075-T6 Al alloy in 3.5wt% NaCl solution, where an Ag/AgCl electrode and Pt are used as the reference and counter electrodes, respectively.

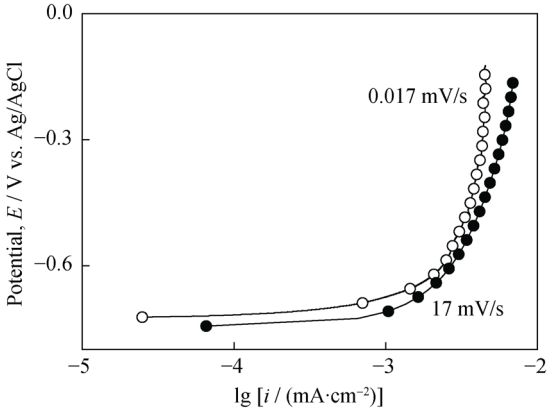

Fig. 7. Fast-slow polarization curves of 7075-T6 Al alloy in 3.5wt% NaCl solution at different scanning rates, where Ag/AgCl and Pt are used as the reference and counter electrodes, respectively.

3.3. SSRT test

SSRT test, as a quick and convenient method, is usually used to estimate the SCC susceptibility of metals and alloys. Fig. 8 shows the strain-stress curves and the corrosion potential during SSRT test for samples in 3.5wt% NaCl solution.

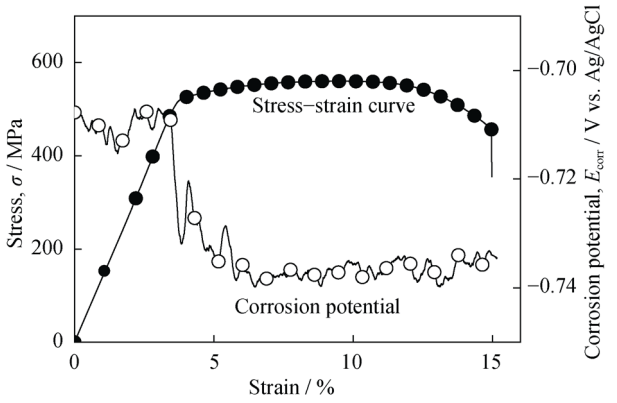

Fig. 8. Strain–stress curve and corrosion potential change during SSRT tests in 3.5wt% NaCl solution, where Ag/AgCl and Pt electrodes are used as the reference and counter electrodes, respectively.

As shown in Fig. 8, the corrosion potential shifts in the negative direction and remains steady at approximately –0.74 V vs. Ag/AgCl after reaching plastic deformation. When the specimen underwent plastic deformation, a substantial amount of fresh metal was exposed in the corrosion solution, resulting in a shift in corrosion potential in the negative direction [25], and then the corrosion was accelerated.

Fig. 9 shows the strain–stress curves of specimens charged in 3.5wt% NaCl solution for 6, 12, and 24 h, respectively. The charging current density was –3 mA/cm^2.

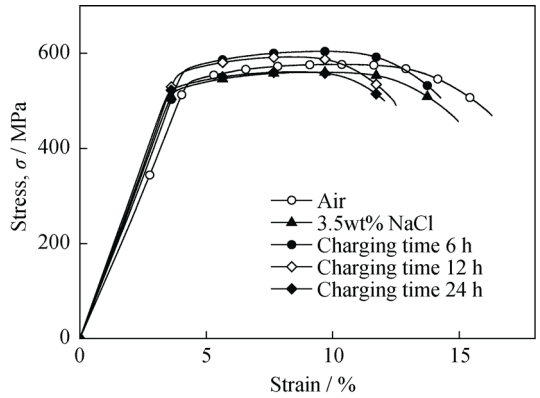

Fig. 9. Strain–stress curves for specimens charged in 3.5wt% NaCl solution for 6, 12, and 24 h, respectively.

As evident in the figure, the elongation to failure (e_f) of the alloy in 3.5wt% NaCl solution is lower than that in air, suggesting that SCC occurs in the 3.5wt% NaCl solution. In addition, the elongation to failure becomes smaller with increasing charging time, indicating that the SCC susceptibility increases.

The SCC susceptibility was also evaluated on the basis of the loss of reduction of area (RA_{loss}), which is defined as follows.

$$RA_{loss} = (RA_{air} - RA_{NaCl}) / RA_{air} \times 100\% \quad (4)$$

An increase in RA_{loss} indicates the increase in SCC susceptibility. The results are presented in Table 2.

Table 2. e_f and RA_{loss} values of specimens

Charging time / h	0	6	12	24
e_f / %	15.1	14.2	12.5	12.0
RA_{loss} / %	5.2	5.8	8.9	14.5

According to the model proposed by Magnin *et al.*, hydrogen atoms can be absorbed by the metal surface [29–30]. Some of these hydrogen atoms diffuse into the bulk, and the remainder can permeate into the metal, resulting in HE. Therefore, an increase in SCC susceptibility is due to an increase in hydrogen entry into the material as a consequence of the longer cathodic charging. The amount of permeated hydrogen was calculated from Figs. 3 and 4 using an integration method. The total hydrogen amount (H_T) was calculated as the sum of hydrogen permeated during cathodic charging (H_C) and during corrosion in the SSRT experiment (H_S), as the following equation:

$$H_T = H_C + H_S \quad (5)$$

The calculated amounts of permeated hydrogen are listed in Table 3.

Table 3. Calculated amounts of hydrogen permeated

Time / h	0	6	12	24
H_C / (10^{-6} mol)	0	4.5	12.2	21.6
H_S / (10^{-6} mol)	0	0.3	0.7	1.1
H_T / (10^{-6} mol)	0	4.8	12.9	22.7

Note: the specimen surface area is 7.1 cm^2.

Tables 2 and 3 show the relationship between H_T and RA_{loss}. RA_{loss} increased with increasing H_T. Zhang *et al.* [31] studied the SCC and HE of an Al–Zn–Mg–Cu alloy and demonstrated that hydrogen decreased the grain boundary strength, resulting in the grain boundary embrittlement. In addition, they observed that the SCC susceptibility increased with increasing cathodic charging time.

Fig. 10 shows the scanning electron microscope (SEM) images of the fracture surface of 7075 aluminum alloy in 3.5wt% NaCl after different cathodic charging times, and the charging current density is –3 mA/cm^2.

Fig. 10(a) shows some typical dimple patterns resulting from ductile fracture. Figs. 10(b)–(d) partially show the cleavage-fractured surfaces. These observations suggested

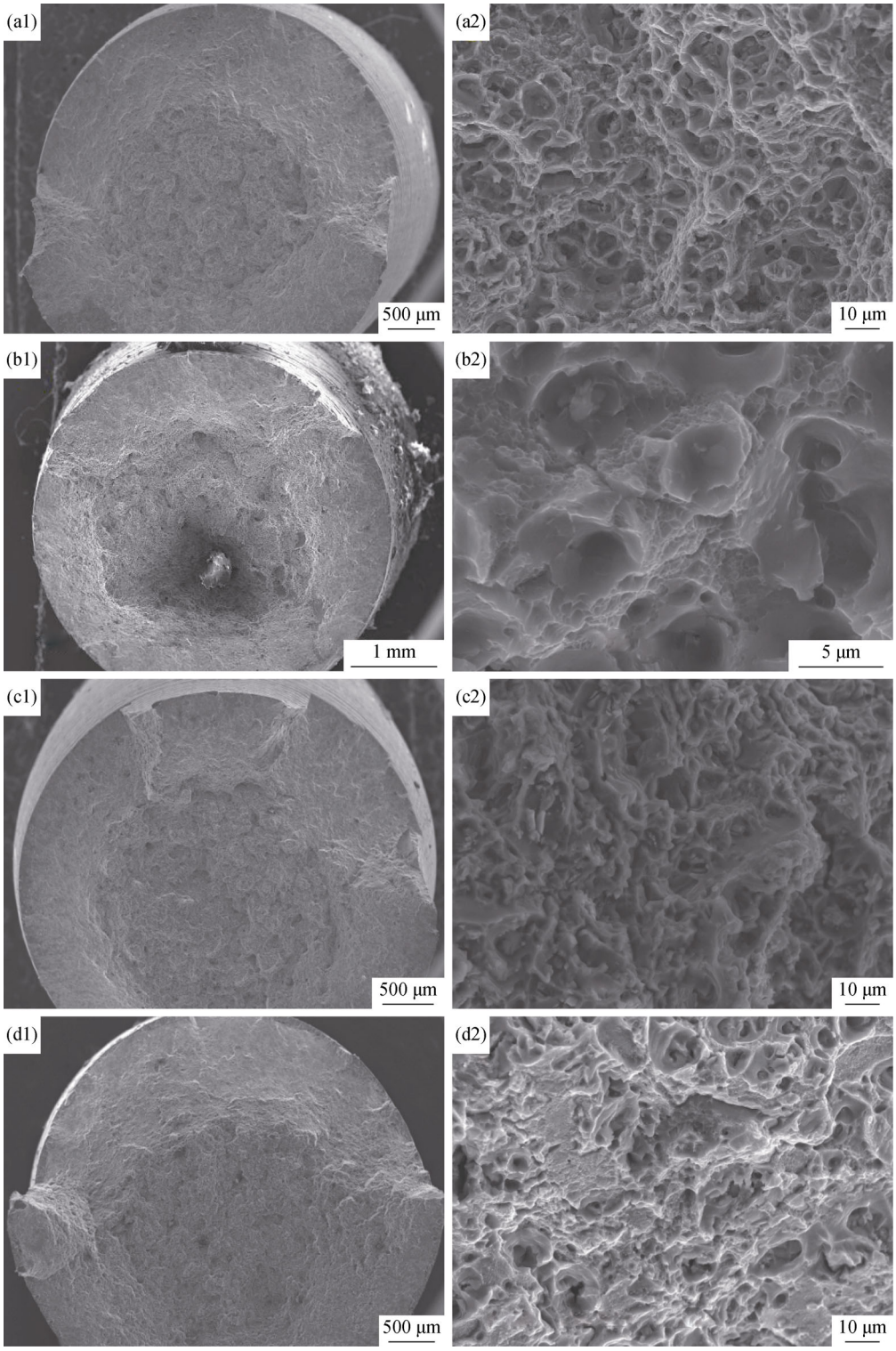

Fig. 10. SEM images of the fracture surface at different charging times: (a) 0 h; (b) 6 h; (c) 12 h; (d) 24 h.

that the specimens were more susceptive to SCC with increasing charging time, which was in agreement with the strain–stress curves in Fig. 9.

To identify the effect of cathodic charging on corrosion, the specimen surface was observed by SEM after 24 h of charging. Fig. 11 shows the SEM images of the specimen surface and the corresponding energy dispersive spectrometer (EDS) analysis results.

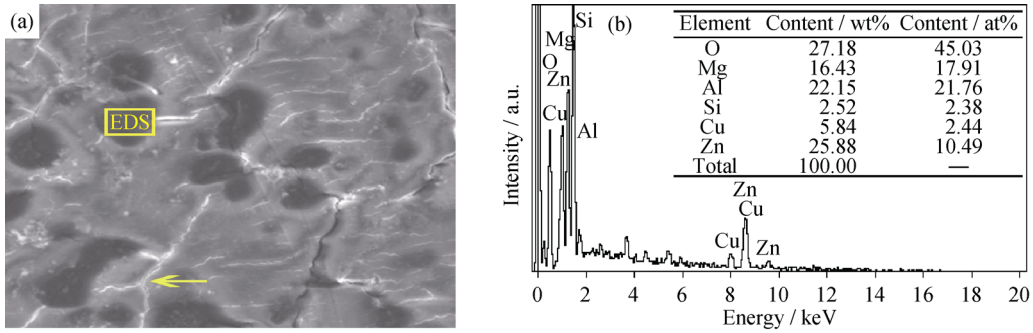

Element	Content / wt%	Content / at%
O	27.18	45.03
Mg	16.43	17.91
Al	22.15	21.76
Si	2.52	2.38
Cu	5.84	2.44
Zn	25.88	10.49
Total	100.00	—

Fig. 11. SEM images (a) and corresponding EDS analysis results (b) for 7075-T6 Al alloy charged for 24 h without tensile testing, where EDS is conducted on rectangular area in Fig. 11(a), and the arrow shows crack near the corrosion pits.

Zhou *et al.* [32] studied the corrosion behavior of aluminum alloys in Na_2SO_4 solution by scanning electrochemical microscopy (SECM) and SEM, and reported that the corrosion area increased and the potential became more negative with increasing immersion time. El-Amoush [33] studied the corrosion behavior of hydrogenated 7075-T6 aluminum alloy and observed that larger pits were formed in the pre-charged specimens during free potential corrosion testing. They also observed that the pit size increased with increasing precharging time.

The aforementioned experimental results indicated that the SCC mechanism of 7075-T6 Al alloy involved the combination of selective corrosion and HE. Song *et al.* [34] concluded that the selective corrosion was Mg-segregation-induced grain boundary embrittlement. However, El-Amoush reported that pitting corrosion occurred during the pre-charging step. As shown in Fig. 11, the similar results were obtained as El-Amoush [33] reported that the corrosion area increased with increasing charging time and some small pits and cracks were formed with increasing charging time. The electrochemical experiments indicated that passivation occurred during anodic polarization; furthermore, the fast-slow polarization curves showed that the specimen exhibited low SCC susceptibility during anodic polarization. To investigate the effect of hydrogen charging on corrosion, the specimen surface was observed by SEM and EDS after being charged for 24 h. As shown in Fig. 11, Selective corrosion plays a dominant role in the pre-charging process, and some corrosion pits are observed on the pre-charged specimens. Some cracks are observed near corrosion pits. EDS analysis reveals that the Mg, O, Zn, and Si contents increase sharply after 24 h of charging. According to Anderatta [35] and Ren [36], the main intermetallics in 7075-T6 Al alloy are $MgZn_2$ and Mg_2Si, and the corrosion potential of $MgZn_2$ and Mg_2Si is more negative than that of Al. In a corrosive environment, anodic dissolution will occur at these two intermetallics. Fig. 12 shows a schematic of the crack-formation process near dissolution pits.

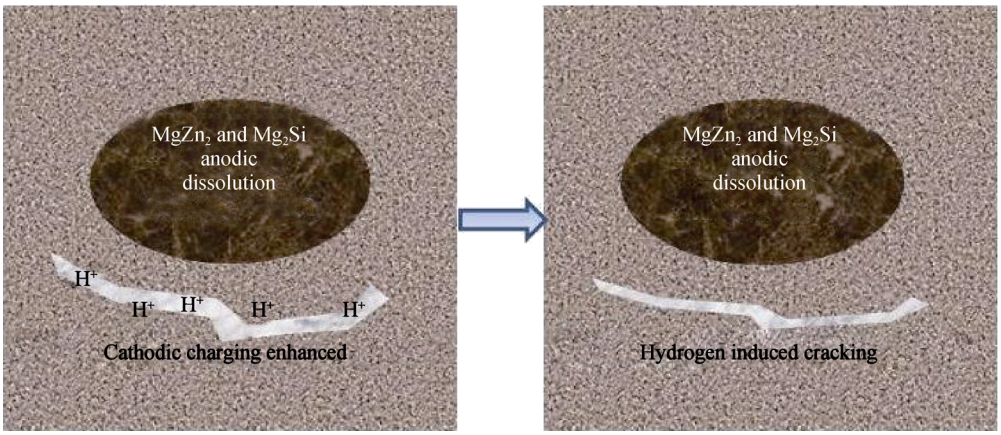

Fig. 12. Schematic illustration of the crack formation process near dissolution pits.

First, $MgZn_2$ and Mg_2Si dissolved under anodic polarization; the hydrogen charging effect was then enhanced near $MgZn_2$ and Mg_2Si under cathodic charging. Finally, cracks were formed. As evident from results in Tables 2 and 3, both the amount of hydrogen generated during the corrosion process and the effect on SCC susceptibility were small. The hydrogen generated during the pre-charging process played a dominant role in SCC susceptibility [37]. These results in-

dicated that pre-charged hydrogen was absorbed by the alloy. In this process, selective corrosion occurred and reduced the grain boundary fracture stress, resulting in grain boundary embrittlement. The small pits might accelerate the stress corrosion crack initiation and propagation, thereby increasing the SCC susceptibility of 7075-T6 Al alloys.

4. Conclusions

(1) The hydrogen permeation current density is successfully measured using a D-S cell after the specimen surface is coated with Ni via a magnetron sputtering method. Hydrogen permeates into the 7075-T6 Al alloy not only during the pre-charging process but also during free potential corrosion tests.

(2) The specimens exhibit SCC in 3.5wt% NaCl solution, and their SCC susceptibility increases with increasing pre-charging time; hydrogen generated during the pre-charging process is observed to play a dominant role in determining SCC susceptibility.

(3) The SCC susceptibility is low during anodic polarization. HE may be the main SCC mechanism of 7075-T6 Al alloy.

(4) Anodic dissolution occurs on intermetallic phases during the cathodic charging process, and the cracking is observed near these dissolution pits.

Acknowledgements

This work was financially supported by the Natural Science Foundation of Jiangsu Province, China (No. BK20141292) and the Foundation of Key Laboratory of Marine Environmental Corrosion and Bio-fouling, Institute of Oceanology, Chinese Academy of Sciences (No. MCKF201412).

References

[1] Y.J. Yan, K.W. Gao, and C.F. Chen, Hydrogen-induced cracking behaviors of Incoloy alloy 825, *Int. J. Miner. Metall. Mater.*, 17(2010), No. 1, p. 58.

[2] Chuanbo Zheng, Guo Yi, Temperature effect on hydrogen permeation of X56 steel, *Mater. Performance,* 50(2011), No. 4, p. 72.

[3] R.H. Jones, D.R. Baer, M.J. Danielson, and J.S. Vetrano, Role of Mg in the stress corrosion cracking of an Al–Mg alloy, *Metall. Mater. Trans. A*, 32(2001), No. 7, p. 1699.

[4] D. Najjar, T. Magnin, and T.J. Warner, Influence of critical surface defects and localized competition between dissolution and hydrogen effects during stress corrosion cracking of a 7050 aluminum alloy, *Mater. Sci. Eng. A.*, 238(1997), No. 2, p. 293.

[5] N. Takano, Hydrogen diffusion and embrittlement in 7075 aluminum alloy, *Mater. Sci. Eng. A*, 483-484(2008), p. 336.

[6] T.M. Yue, L.J. Lan, C.F. Dong, and C.P. Chan, Stress corrosion cracking behaviour of laser treated aluminum alloy 7075 using a slow strain rate test, *Mater. Sci. Technol.*, 21(2005), No. 8, p. 961.

[7] N. Winzer, A. Atrens, W. Dietzel, V.S. Raja, G. Song, and K.U. Kainer, Characterisation of stress corrosion cracking (SCC) of Mg–Al alloys, *Mater. Sci. Eng. A.*, 488(2008), No. 1-2, p. 339.

[8] E.U. Lee, A.K. Vasudevan, and G. Glinka, Environmental effects on low cycle fatigue of 2024-T351 and 7075-T651 aluminum alloys, *Int. J. Fatigue*, 31(2009), No. 11-12, p. 1938.

[9] A. Thakur, R. Raman, and S.N. Malhotra, Hydrogen embrittlement studies of aged and retrogressed-reaged Al–Zn–Mg alloys, *Mater. Chem. Phys.*, 101(2007), No. 2-3, p. 441.

[10] C.F. Dong, K. Xiao, Z.Y. Liu, W.J. Yang, and X.G. Li, Hydrogen induced cracking of X80 pipeline steel, *Int. J. Miner. Metall. Mater.*, 17(2010), No. 5, p. 579.

[11] G. Kotsikos, J.M. Sutcliffe, and N.J.H. Holroyd, Hydrogen effects in the corrosion fatigue behaviour of the white zone of 7xxx series aluminum alloy welds, *Corros. Sci.*, 42(2000), No. 1, p. 17.

[12] Al.Th. Kermanidis, P.V. Petroyiannis, and Sp.G. Pantelakis, Fatigue and damage tolerance behaviour of corroded 2024 T351 aircraft aluminum alloy, *Theor. Appl. Fract. Mech.*, 43(2005), No. 1, p. 121.

[13] Y. Zhang, R.G. Song, and P.H. Tang, Hydrogen embrittlement susceptibility and Mg–H interaction in 7075 aluminum alloy, *J. Chin. Soc. Corros. Prot.*, 30(2010), No. 5, p. 364.

[14] Y. Reda, R. Abdel-Karim, and I. Elmahallawi, Improvements in mechanical and stress corrosion cracking properties in Al-alloy 7075 via retrogression and reaging, *Mater. Sci. Eng. A.*, 485(2008), No. 1-2, p. 468.

[15] H. Kamoutsi, G.N. Haidemenopoulos, V. Bontozoglou, and S. Pantelakis, Corrosion-induced hydrogen embrittlement in aluminum alloy 2024, *Corros. Sci.*, 48(2006), No. 5, p. 1209.

[16] A.M. Thad, K. Paul, and D. Andrew, Evaluation of oxidation and hydrogen permeation in Al-containing stainless steel alloys, *Mater. Sci. Eng. A*, 424(2006), No. 1-2, p. 33.

[17] M.J. Danielson, Use of the Devanathan–Stachurski cell to measure hydrogen permeation in aluminum alloys, *Corros. Sci.*, 44(2002), No. 4, p. 829.

[18] A.I. Onuchukwu and S. Trasatti, Hydrogen permeation into aluminum alloy 1060 as a results of corrosion in alkaline medium. Basic features of the process, *Electrochim. Acta*, 33(1988), No. 10, p. 1425.

[19] C. Nishimura, T. Ozaki, M. Komaki, and Y. Zhang, Hydrogen permeation and transmission electron microscope observations of V–Al alloys, *J. Alloys Compd.,* 356-357(2003), p. 295.

[20] Y.J. Ouyang, G. Yu, A.L. Ou, L. Hu, and W.J. Xu, Double electrolyte sensor for monitoring hydrogen permeation rate in

steels, *Corros. Sci.*, 53(2011), No. 6, p. 2247.

[21] C.B. Zheng, G. Yi, Y.M. Gao, and K. Zhang, Hydrogen permeation and stress corrosion cracking sensitivity of 7075-T6 Al alloy in marine environment, *Chin. J. Nonferrous Met.*, 23(2013), No. 8, p. 2118.

[22] F.D. Fischer, G. Mori, and J. Svoboda, Modelling the influence of trapping on hydrogen permeation in metals, *Corros. Sci.*, 76(2013), p. 382.

[23] R.J. Gest and A.R. Troiano, Stress corrosion and hydrogen embrittlement in an aluminum alloy, *Corrosion*, 30(1974), No. 8, p. 274.

[24] M. Kupka, K. Stępień, and B. Łosiewicz, Effect of plastic working on hydrogen permeability in an FeAl-based alloy, *J. Alloys Compd.*, 482(2009), No. 1-2, p. 371.

[25] C.B. Zheng, Y.L. Huang, Q. Yu, C.Y. Huo, and Y.L. Huang, Effect of H_2S on stress corrosion cracking and hydrogen permeation behaviour of X56 grade steel in atmospheric environment, *Corros. Eng. Sci. Technol.*, 44(2009), No. 2, p. 96.

[26] S.J. Chen, Q.M. Yuan, J.P. He, and X.L. Liu, Potential fluctuations of 7075 aluminum alloy under thin electrolyte layers, *J. Electrochem.*, 11(2005), No. 2, p. 167.

[27] G.D. Sulka and P. Jóźwik, Electrochemical behavior of Ni_3Al-based intermetallic alloys in NaOH, *Intermetallics.*, 19(2011), No. 7, p. 974.

[28] Y. Liu, Y.L. Huang, and B.R. Hou, Study on stress corrosion behavior of 16M steel with ZnAl hot-dipped coating in seawater, *China Surf. Eng.*, 18(2005), No. 3, p. 45.

[29] W.Y. Chu, K.W. Gao, L.J. Qiao, and Y. Zhang, An investigation of corrosion-induced stress during SCC, *J. Univ. Sci. Technol. Beijing.*, 10(2003), No. 1, p. 1.

[30] E. Lunarska and O. Chernyayeva, Effect of the self-induced strain on the hydrogen permeation through Al, *Int. J. Hydrogen Energy*, 31(2006), No. 2, p. 237.

[31] G.K. Zhang, X.L. Wang, Y.F. Xiong, Y. Shi, J.F. Song, and D.L. Luo, Mechanism for adsorption, dissociation and diffusion of hydrogen in hydrogen permeation barrier of α-Al_2O_3: a density function theory study, *Int. J. Hydrogen Energy*, 38(2013), No. 2, p. 1157.

[32] H.R. Zhou, X.G. Li, C.F. Dong, K. Xiao, and T. Li, Corrosion behavior of aluminum alloys in Na_2SO_4 solution using the scanning electrochemical microscopy technique, *Int. J. Miner. Metall. Mater.*, 16(2009), No. 1, p. 84.

[33] A.S. El-Amoush, Erratum to "An investigation of mechanical degradation of AlMg1SiCu aluminum alloy by hydrogen", *J. Alloys Compd.*, 440(2007), No. 1-2, p. 380.

[34] R.G. Song, W. Dietzel, B.J. Zhang, W.J. Liu, M.K. Tseng, and A. Atrens, Stress corrosion cracking and hydrogen embrittlement of an Al–Zn–Mg–Cu alloy, *Acta Mater.*, 52(2004), No. 16, p. 4727.

[35] F. Anderatta, H. Terryn, and J.H.W. de Wit, Corrosion behaviour of different tempers of AA7075 aluminium alloy, *Electrochim. Acta*, 49(2004), No. 17-18, p. 2851.

[36] X.P. Ren, F.F. Zhang, Q.M. Guo, H.L. Hou, and Y.Q. Wang, Hydrogen absorption behavior of TA15 alloy, *Int. J. Miner. Metall. Mater.*, 18(2011), No. 2, p. 210.

[37] H. Sheng, C.F. Dong, K. Xiao, X.G. Li, and L. Lu, Anodic dissolution of a crack tip at AA 2024-T351 in 5wt% NaCl solution, *Int. J. Miner. Metall. Mater.,* 19(2012), No. 10, p. 939.